Supporting Information

Theoretical Exploration of Nitrogen Fixation Mechanism of Two-dimensional Dual-Metal $TM_1TM_2@C_9N_4$ Electrocatalysts

Jinxin Sun,[1‖] Peng Xia,[1‖] Yuxing Lin,[1‖] Yunfan Zhang,[1] Anjie Chen,[1] Li Shi,[2] Yongjun Liu,[1] Xianghong Niu,[3*] Ailei He,[1*] Xiuyun Zhang[1*]

[1]College of Physics Science and Technology, Yangzhou University, Yangzhou 225002, China

[2]State Key Laboratory of Organic Electronics and Information Displays & Institute of Advanced Materials (IAM), Jiangsu National Synergetic Innovation Center for Advanced Materials (SICAM), School of Materials Science and Engineering, Nanjing University of Posts and Telecommunications Nanjing 210023, China

[3]New Energy Technology Engineering Laboratory of Jiangsu Province & School of Science, Nanjing University of Posts and Telecommunications, Nanjing, 210023, China

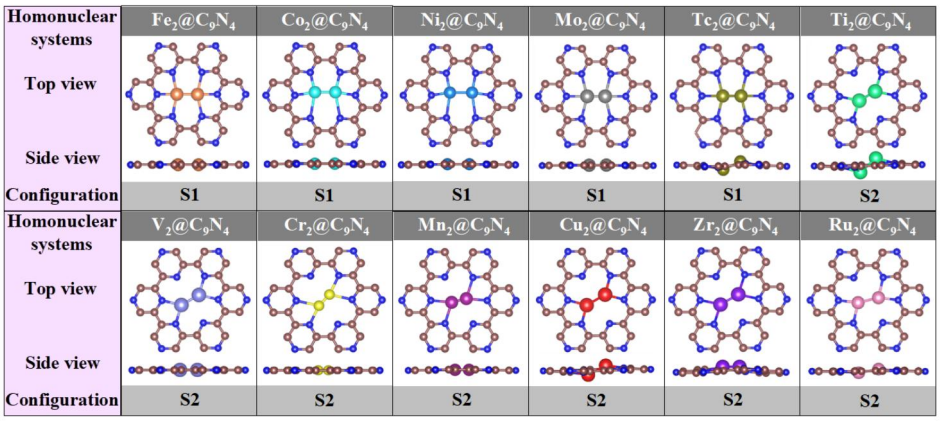

Fig. S1. The top and side view of the optimized structures of homonuclear dual-metal atom $TM_1TM_2@C_9N_4$s.

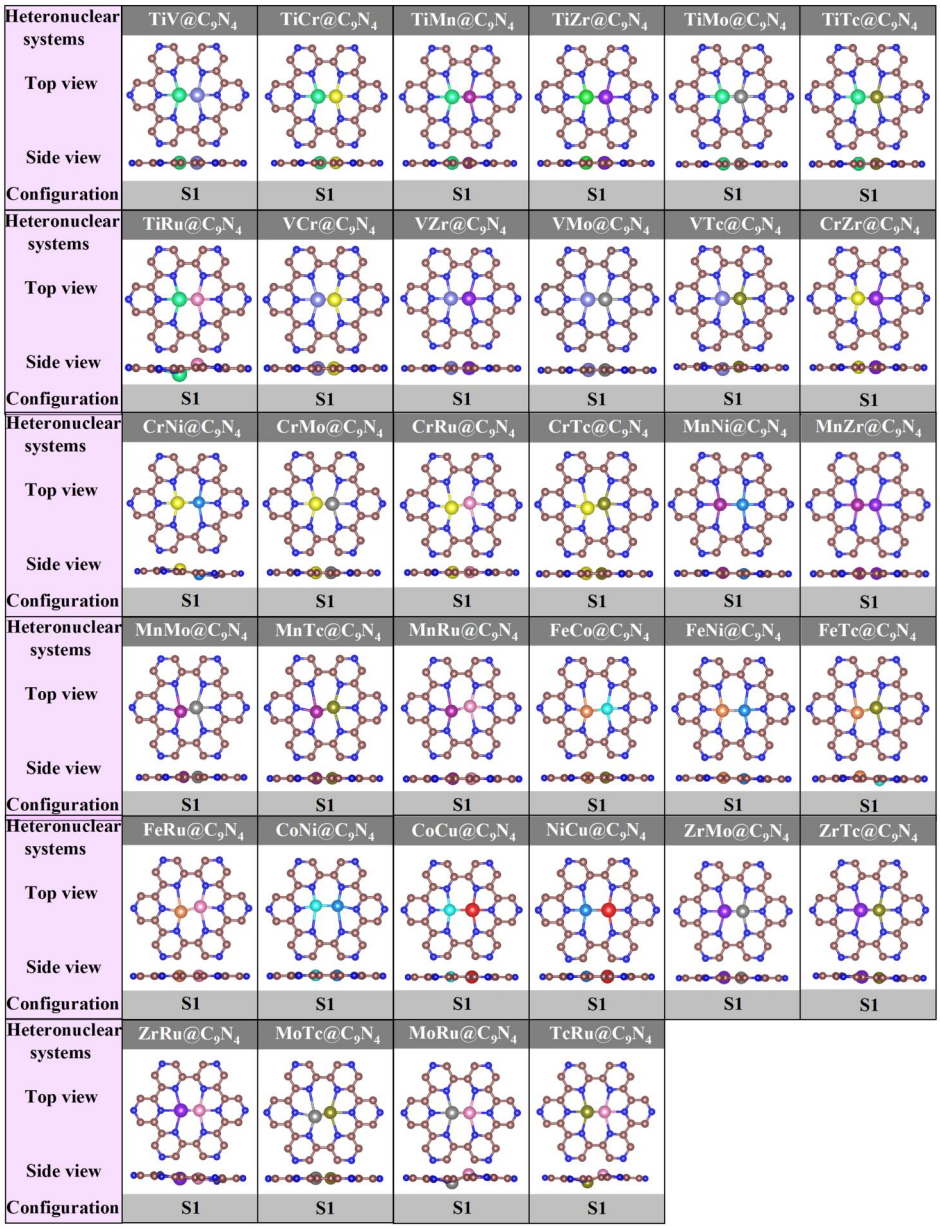

Fig. S2. Top and side view of the optimized structures of heteronuclear dual-metal atom $TM_1TM_2@C_9N_4$ with S1 configuration.

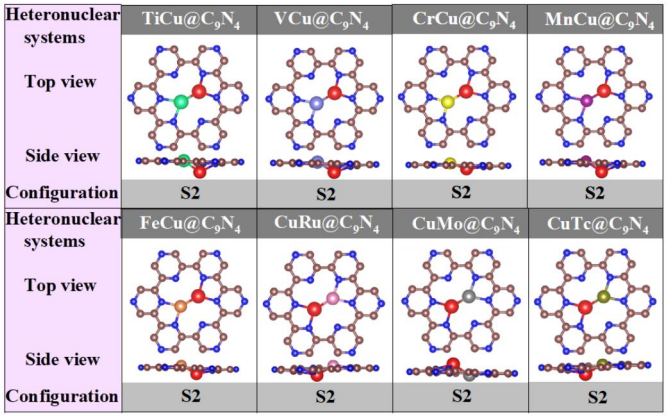

Fig. S3. Top and side view of the optimized structures of heteronuclear dual-metal atom $TM_1TM_2@C_9N_4$ with S2 configuration.

Heteronuclear systems	$TiFe@C_9N_4$	$TiCo@C_9N_4$	$TiNi@C_9N_4$	$VMn@C_9N_4$	$VFe@C_9N_4$	$VCo@C_9N_4$
Top view / Side view	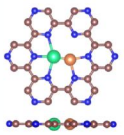	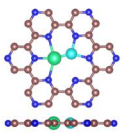	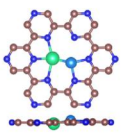	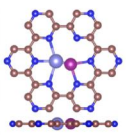	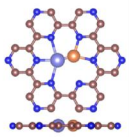	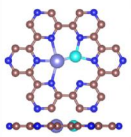
Configuration	S3	S3	S3	S3	S3	S3
Heteronuclear systems	$VNi@C_9N_4$	$VRu@C_9N_4$	$CrMn@C_9N_4$	$CrFe@C_9N_4$	$CrCo@C_9N_4$	$MnFe@C_9N_4$
Top view / Side view	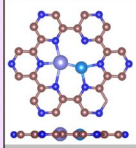	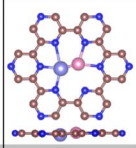	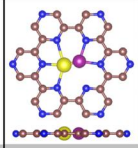	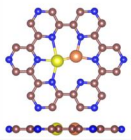	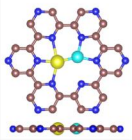	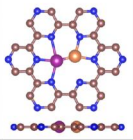
Configuration	S3	S3	S3	S3	S3	S3
Heteronuclear systems	$MnCo@C_9N_4$	$FeZr@C_9N_4$	$FeMo@C_9N_4$	$CoZr@C_9N_4$	$CoMo@C_9N_4$	$CoRu@C_9N_4$
Top view / Side view	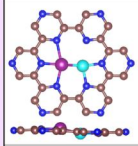	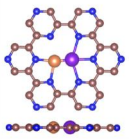	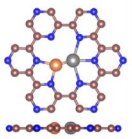	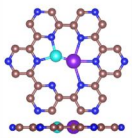	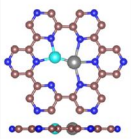	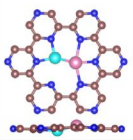
Configuration	S3	S3	S3	S3	S3	S3
Heteronuclear systems	$CoTc@C_9N_4$	$NiZr@C_9N_4$	$NiMo@C_9N_4$	$NiTc@C_9N_4$	$NiRu@C_9N_4$	$CuZr@C_9N_4$
Top view / Side view	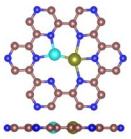	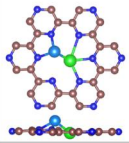	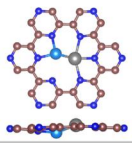	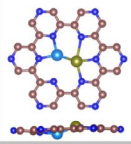	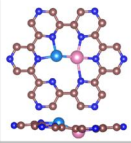	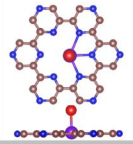
Configuration	S3	S3	S3	S3	S3	None

Fig. S4. Top and side view of the optimized structures of heteronuclear dual-metal atom $TM_1TM_2@C_9N_4$ with S3 configuration.

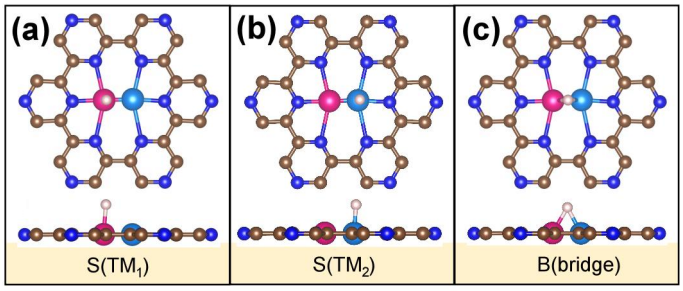

Fig. S5**.** Top and side views of (a) S_1, (b) S_2 and (c) S_3 configuration of *H absorbed in active centers of $TM_1TM_2@C_9N_4$.

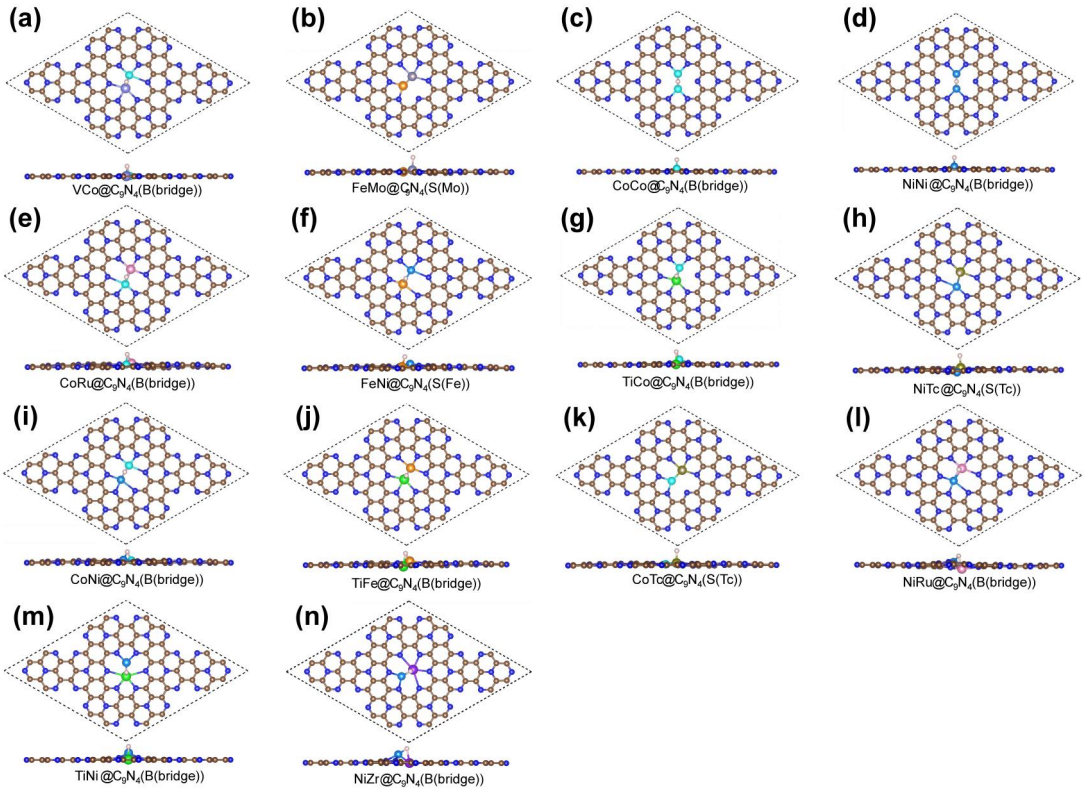

Fig. S6. Optimized geometries of H* adsorbed on 14 $TM_1TM_2@C_9N_4$ (TM_1TM_2= FeMo, VCo, CoCo, NiNi, CoRu, FeNi, TiCo, NiTc, CoNi, TiFe, CoTc, NiRu, TiNi, and NiZr). The brown, blue, pink balls represent C, N, and H atoms, respectively.

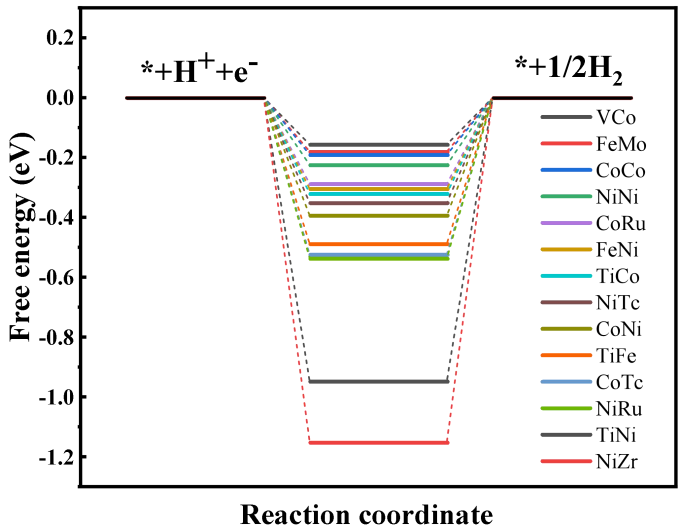

Fig. S7. Free energy diagrams of HER on $TM_1TM_2@C_9N_4$ (TM_1TM_2=FeMo, VCo, CoCo, NiNi, CoRu, FeNi, TiCo, NiTc, CoNi, TiFe, CoTc, NiRu, TiNi, and NiZr).

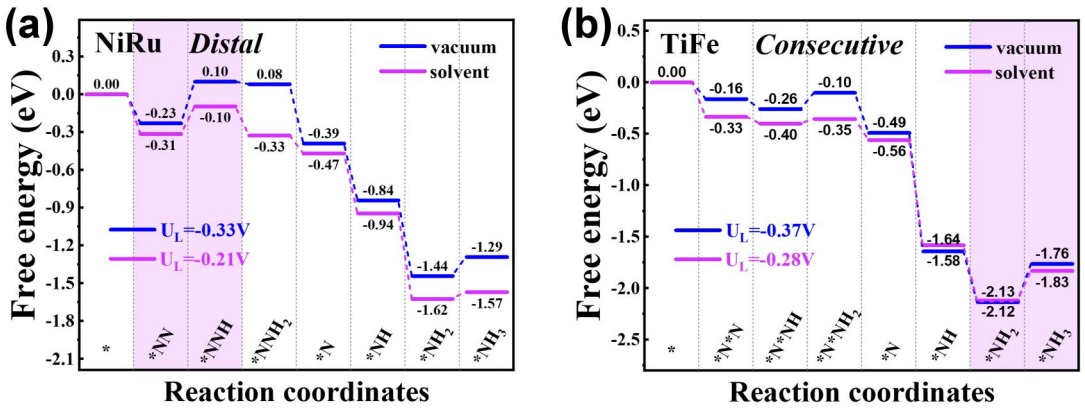

Fig. S8. Free energy diagrams of NRR on (a) NiRu@C_9N_4, and (b) TiFe@C_9N_4 along distal mechanism. Blue and pink lines indicate free energy change for NRR in vacuum and solvent environment, respectively.

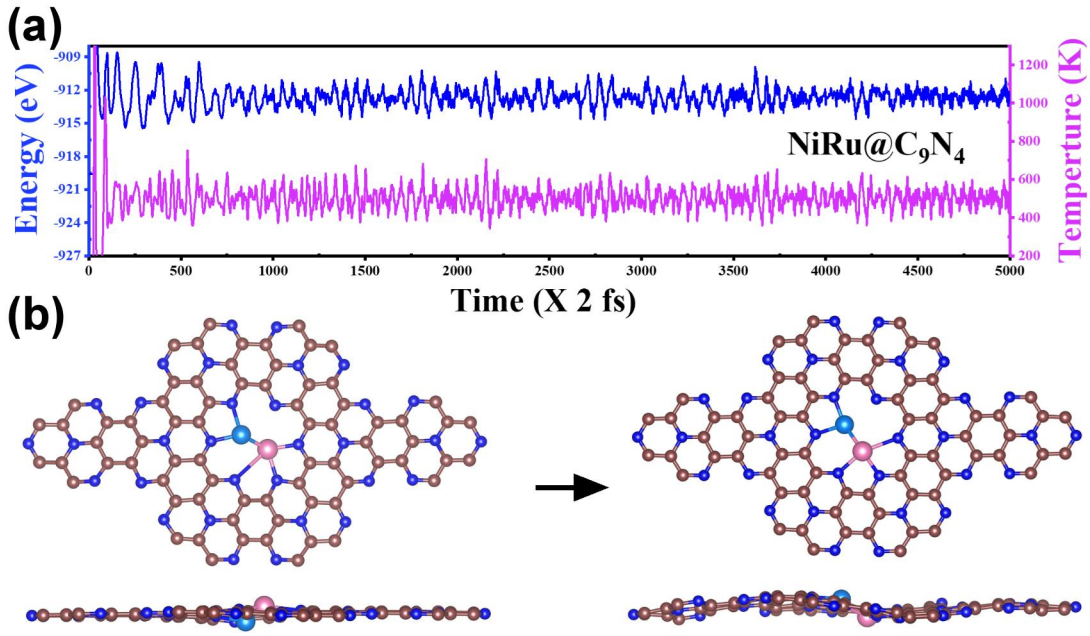

Fig. S9. (a) Variations of temperature and energy against the time for AIMD simulations of NiRu@C_9N_4. (b) top and side views of the configuration of NiRu@C_9N_4 before and after AIMD simulation. The simulation was performed under 500 K for 10 ps with a time step of 2 fs.

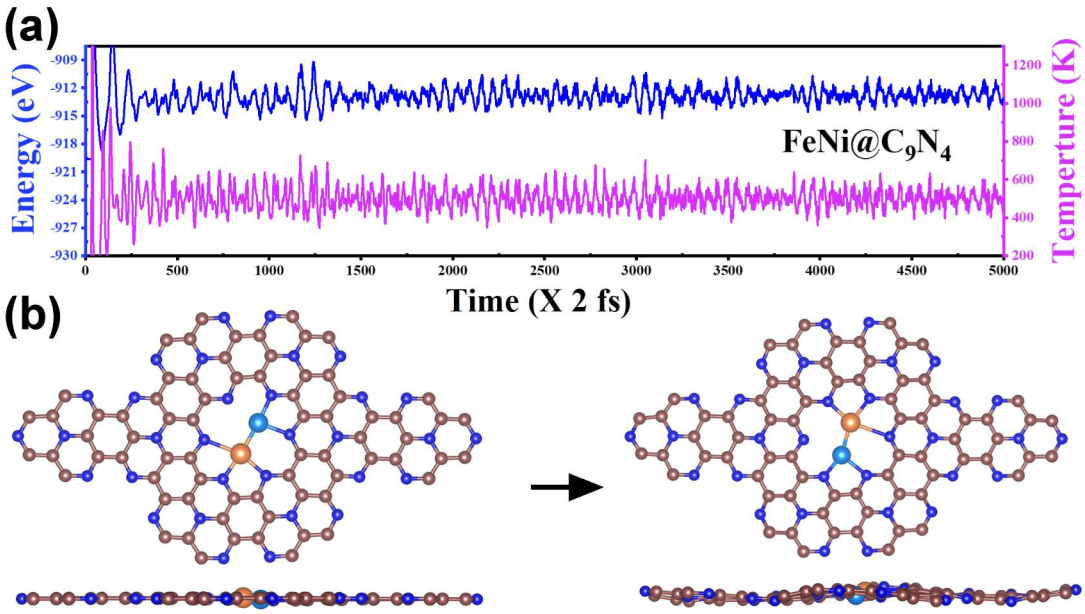

Fig. S10. (a) Variations of temperature and energy against the time for AIMD simulations of FeNi@C_9N_4. (b) Top and side views of the configuration of FeNi@C_9N_4 before and after AIMD simulation. The simulation was performed under 500 K for 10 ps with a time step of 2 fs.

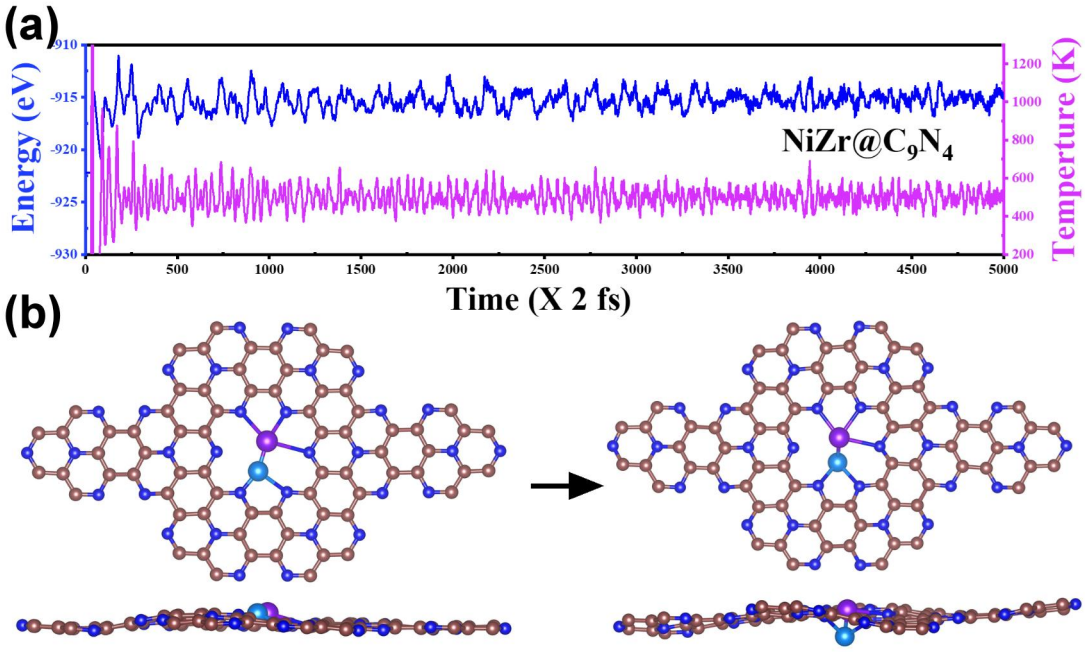

Fig. S11. (a)Variations of temperature and energy against the time for AIMD simulations of NiZr@C_9N_4. (b) Top and side views of the configuration of NiZr@C_9N_4 before and after AIMD simulation. The simulation was performed under 500 K for 10 ps with a time step of 2 fs.

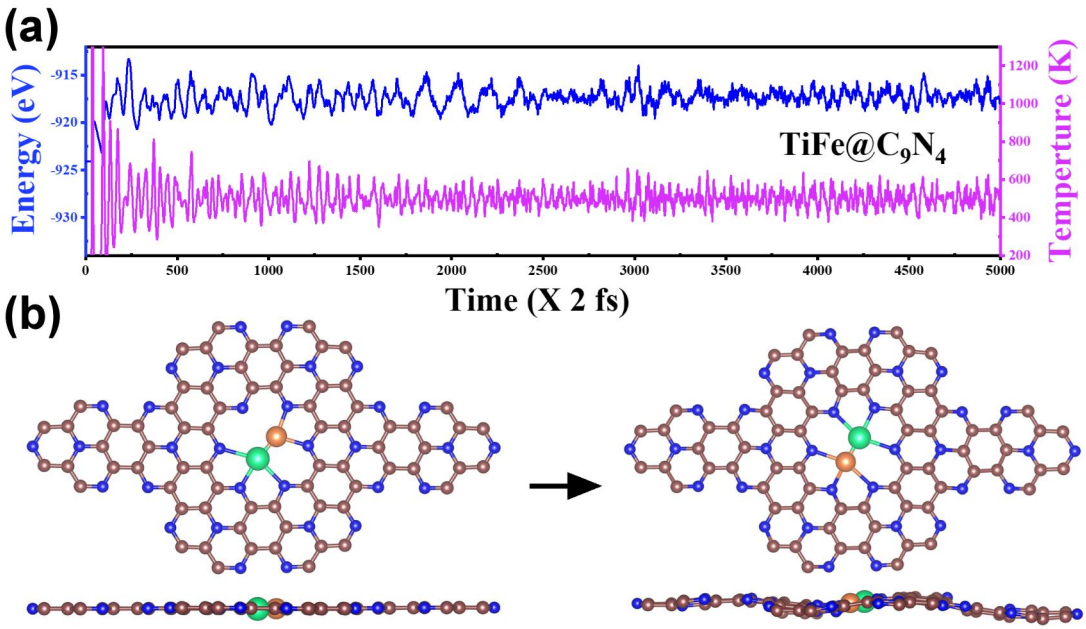

Fig. S12. (a)Variations of temperature and energy against the time for AIMD simulations of TiFe@C_9N_4. (b)Top and side views of the configuration of TiFe@C_9N_4 before and after AIMD simulation. The simulation was performed under 500 K for 10 ps with a time step of 2 fs.

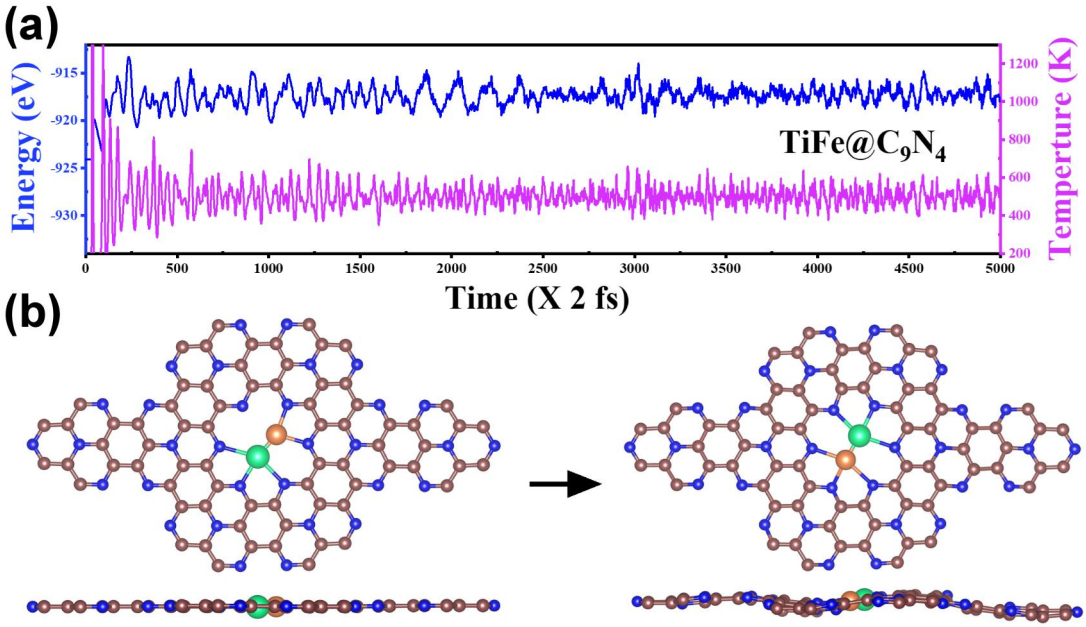

Fig. S13. (a)Variations of temperature and energy against the time for AIMD simulations of TiNi@C_9N_4. (b)Top and side views of the configuration of TiNi@C_9N_4 before and after AIMD simulation. The simulation was performed under 500 K for 10 ps with a time step of 2 fs.

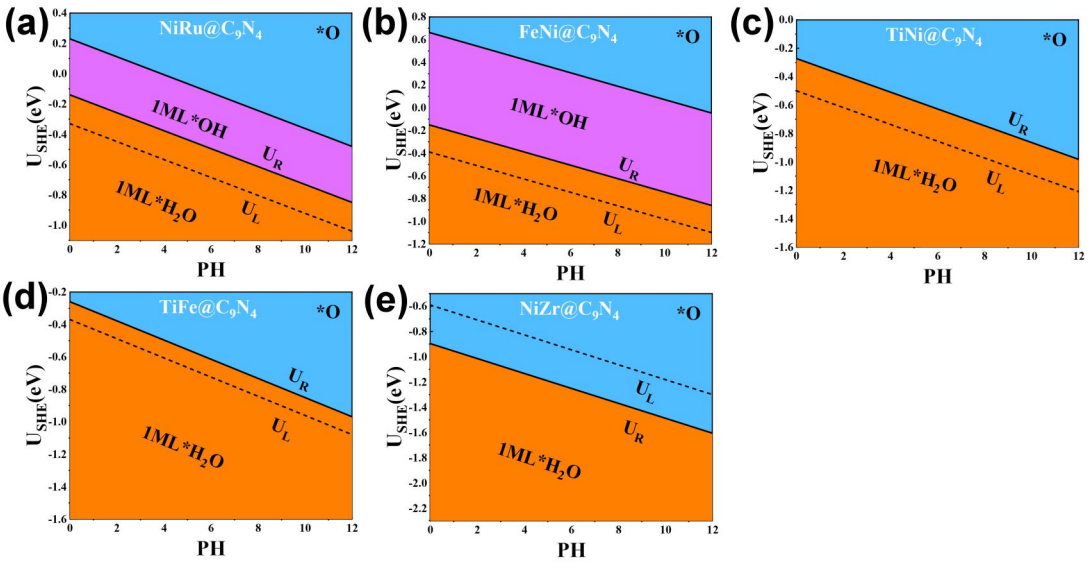

Fig. S14. Surface Pourbaix diagrams on the 5 $TM_1TM_2@C_9N_4$ (TM_1TM_2=NiRu, FeNi, TiNi, TiFe, and NiZr). The thermodynamically stable states of the surface under relevant reversible hydrogen electrode (RHE) and pH values are highlighted by blue (for *O), pink (for *OH), and orange (for *H_2O), respectively.

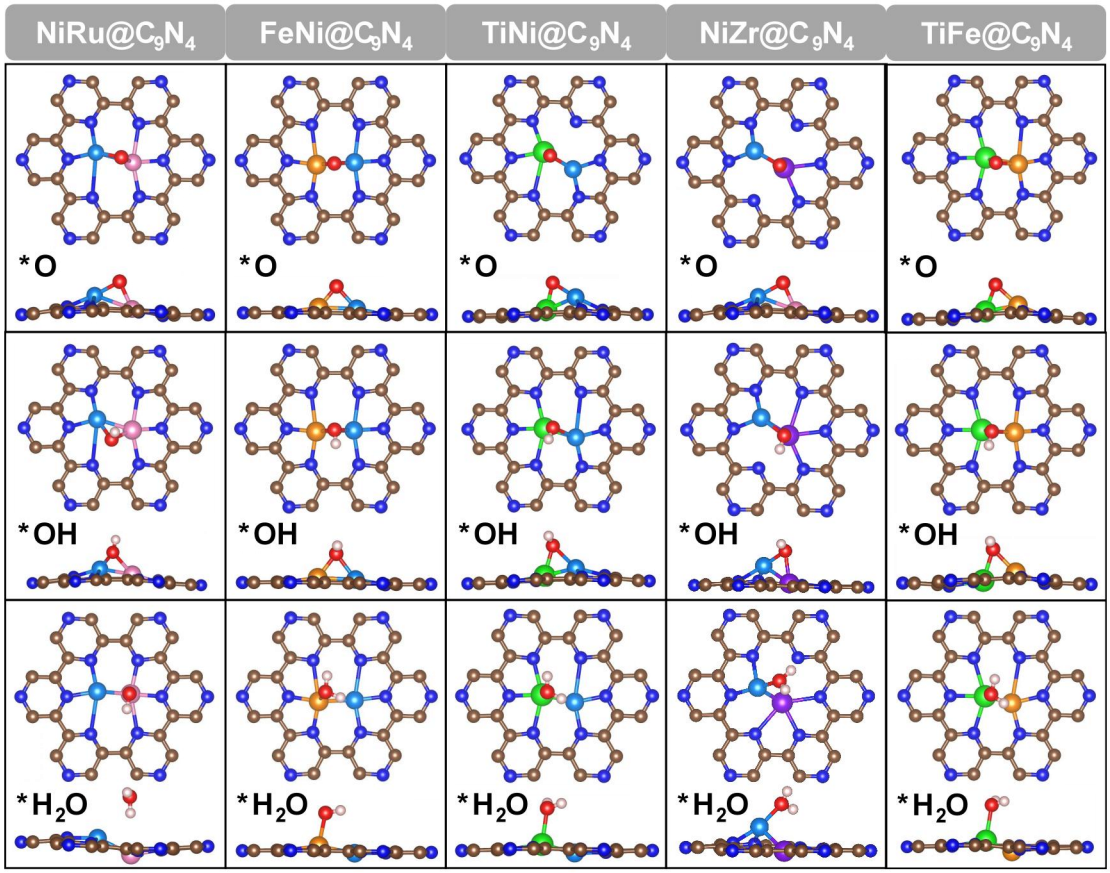

Fig. S15. Optimized Structures of oxygen atom/hydroxyl/single water at the 1ML on the 5 $TM_1TM_2@C_9N_4$ (TM_1TM_2=NiRu, FeNi, TiNi, TiFe, and NiZr).